Numerical study on the effects of intake charge on oxy-fuel combustion in a dual-injection spark ignition engine at economical oxygen-fuel ratios

Xiang Li [a], Yiqiang Pei [b], Zhijun Peng [a,*], Tahmina Ajmal [a], Khaqan-Jim Rana [a], Abdel Aitouche [c, d], Raouf Mobasheri [c, d]

[a] School of Computer Science and Technology, University of Bedfordshire, Luton, UK

[b] State Key Laboratory of Engines, Tianjin University, Tianjin, China

[c] Univ. Lille, CNRS, Centrale Lille, UMR 9189 - CRIStAL - Centre de Recherche en Informatique Signal et Automatique de Lille, F-59000 Lille, France

[d] Junia, Smart Systems and Energies, F-59000 Lille, France

*Corresponding author:

Zhijun Peng, School of Engineering, University of Lincoln, Lincoln, LN6 7TS, UK

Email: jpeng@lincoln.ac.uk

Abstract

In order to decrease Carbon Dioxide (CO_2) emissions, Oxy-Fuel Combustion (OFC) technology with Carbon Capture and Storage (CCS) is being developed in Internal Combustion Engine (ICE). In this article, a numerical study about the effects of intake charge on OFC was conducted in a dual-injection Spark Ignition (SI) engine, with Gasoline Direct Injection (GDI), Port Fuel Injection (PFI) and P-G (50% PFI and 50% GDI) three injection strategies. The results show that under OFC with fixed Oxygen Mass Fraction (OMF) and intake temperature, the maximum Brake Mean Effective Pressure (BMEP) is each 5.671 bar, 5.649 bar and 5.646 bar for GDI, P-G and PFI strategy, which leads to a considerable decrease compared to Conventional Air Combustion (CAC). φ_{CA50}, θ_F and θ_C of PFI are the lowest among three injection strategies. With intake temperature increases from 298 K to 378 K, the reduction of BMEP can be up to 12.68%, 12.92% and 12.75% for GDI, P-G and PFI, respectively. Meantime, there is an increase of about 3% in Brake Specific Fuel Consumption (BSFC) and Brake Specific Oxygen Consumption (BSOC). Increasing OMF can improve the performance of BMEP and BSFC, and the trend is more apparent under GDI strategy. Besides, an increasing tendency can be observed for cylinder pressure and in-cylinder temperature under all injection strategies with the increase of OMF.

Keywords

Oxy-Fuel Combustion (OFC); Dual-injection Spark Ignition (SI) engine; Intake temperature; Oxygen Mass Fraction (OMF); Simulation

1. Introduction

In recent decades, one of the most serious concerns in the world is global warming. It is closely linked to Carbon Dioxide (CO_2) emissions, which is the most significant long-lived Greenhouse Gas (GHG) in the atmosphere. Carbon neutrality has become an urgent appeal to slow the climate crisis [1][2][3][4][5][6]. Several relevant advanced technologies, such as battery electric, hybrid electric, plug-in hybrid electric and fuel-cell electric, have been used in passenger cars, demonstrating a good ability to decrease even eliminate CO_2 emissions [7][8]. However, due to the high cost and low torque output, these technologies are difficult to be applied in non-road machinery, such as vessels and boats.

In order to help achieve carbon neutrality from fossil fuel powered non-road machinery, Oxy-Fuel Combustion (OFC) technology has been widely applied in generating stations and Internal Combustion Engine (ICE) as a valid method for Carbon Capture and Storage (CCS). Yaverbaum [9] first introduced OFC in 1977, which great advantage is capable of removing nitrogen during combustion process. The chemical reaction of OFC can be illustrated in equation (1).

$$C_xH_y + \left(x + \frac{y}{4}\right) O_2 \rightarrow xCO_2 + \frac{y}{2} H_2O \quad (1)$$

Figure 1 shows a complete schematic of OFC technology with CCS in ICE. Pure oxygen is introduced instead of air for fuel combustion, meantime some of the exhaust gas is recirculated to back to cylinders during a typical OFC working process. Afterwards, the excess CO_2 can be separated, captured and stored by water separator, compressor and CO_2 storage tank in the exhaust gas treatment system. Besides, the differences in physicochemical properties between CO_2 and nitrogen are listed in Table 1, which has a major influence on combustion characteristics of OFC and Conventional Air Combustion (CAC) [10][11][12].

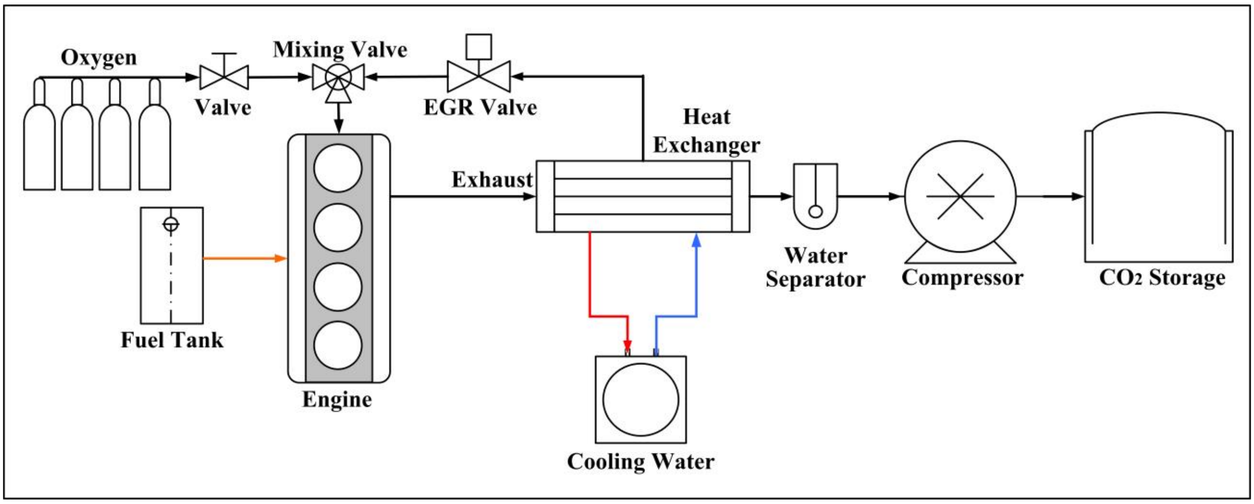

Figure 1. Schematic of OFC technology with CCS in the application of ICE

Table 1. Physicochemical properties of CO_2 and nitrogen at 1000 k and 0.1 MPa [10][11][12]

Property	CO_2	nitrogen	Ratio (CO_2/nitrogen)
Molecular weight	44	28	1.57
Density (kg/m^3)	0.5362	0.3413	1.57
Kinematic viscosity (m^2/s)	7.69e-5	1.2e-4	0.631

Specific heat capacity (kJ/kg K)	1.2343	1.1674	1.06
Thermal conductivity (W/m K)	7.057e-2	6.599e-2	1.07
Thermal diffusivity (m^2/s)	1.1e-4	1.7e-4	0.644
Mass diffusivity of O_2 (m^2/s)	9.8e-5	1.3e-4	0.778
Prandtl number	0.7455	0.7022	1.06
Emissivity and absorptivity	>0	~0	-

In terms of Compression Ignition (CI) engines, OFC technology was initially implemented in the Closed Cycle Diesel Engine (CCDE), which exhaust gas can be recirculated after combustion-produced by-products are separated and removed from the inert working fluid [13][14]. Subsequently, Zhang and Zhu [15] outlined CCDE's working principle and studied the effects of various influencing factors on engine performance. Wu et al. [16][17][18] demonstrated that the combustion performance of CCDE could be improved with by changing intake components. Mobasheri et al. [19][20] numerically investigated the effects of OFC on engine operating conditions and combustion characteristics in Homogenous Charge Compression Ignition (HCCI) engine under different diluent strategies. Li et al. [21] conducted a feasibility study of OFC implementation in a practical diesel engine at economical oxygen-fuel ratios by computer simulation.

Regarding the study of OFC in Spark Ignition (SI) engines, Bilger [22] firstly proposed a novel OFC method named Internal Combustion Rankine Cycle (ICRC), which feature is that preheated water is directly injected to cylinder for controlling combustion process. Wu et al. [23][24][25][26][27][28][29] applied ICRC method to practical Port Fuel Injection (PFI) SI engines fuelled with propane under operating conditions of oxygen volume fraction from 40% to 55%. These studies revealed that engine performance under OFC mode could be improved by optimising operating parameters, such as oxygen fraction, water injection, etc.

Nowadays, Gasoline Direct Injection (GDI) technology has been widely adopted as a common engine configuration and a hot spot on the academia and industry [30][31][32][33][34][35]. In 2005, an advanced technology named dual-injection, which schematic is shown in Figure 2, was commercially applied to SI engines by Toyota [36]. With the combination of GDI and PFI's advantages, dual-injection technology of SI engine has attracted more researchers in recent years. Ikoma et al. [36] studied fuel economy on the Environmental Protection Agency (EPA) cycle from a V-6 3.5-litre dual-injection SI engine fuelled with gasoline. Stein et al. [37] applied DI of E85 (a blend of 15% gasoline and 85% ethanol) plus PFI of gasoline on a SI engine. It is found that a higher compression ratio and boost level can be achieved due to effective knock suppression. Audi stated that optimising fuel injection and complying future emission limits can be achieved by exploring the potential of dual-injection technology in SI engines [38]. Daniel et al. [39][40][41] investigated the fuel efficiency, CO, NO_X, HC and particulate emissions by using PFI of gasoline plus Direct Injection (DI) of various fuels such as gasoline, ethanol and 2,5-dimethylfuran. Zhang et al. [42][43][44] and Wang et al. [45][46][47] also made significant contributions to the research of dual-injection SI engines in emission reduction and fuel economy improvement.

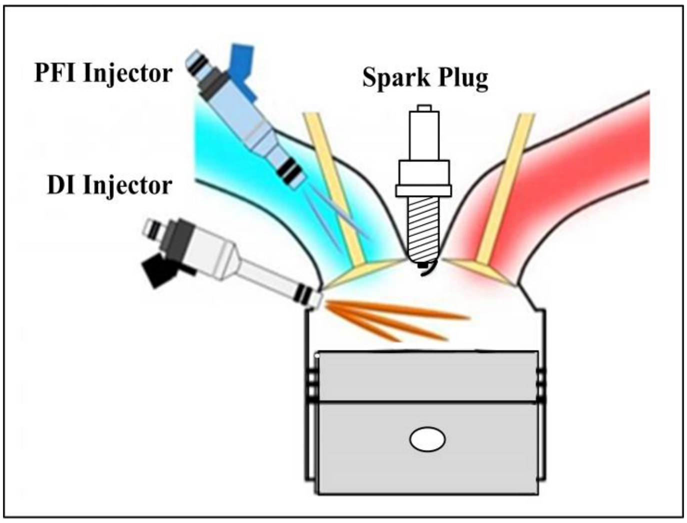

Figure 2. Schematic of a dual-injection system in SI engine

As reviewed above, previous literature about the implementation of OFC in SI engines mainly focused on PFI engines with intake charge of high oxygen fractions. However, the investigation of OFC technology in dual-injection SI engines has not been reported before. Furthermore, as intake charge management affects the quantity, composition, temperature and pressure of the cylinder's contents during the combustion process, it significantly impacts engine operating behaviour. Hence, the effects of intake charge on OFC in a dual-injection SI engine is necessary to be investigated.

The work in this article is part of an ongoing research project named 'RIVER', which is an international collaborative research project funded by the Interreg North-West Europe. OFC technology is implemented and investigated for the powertrain of inland waterway vessels to help achieve zero-carbon emissions for meeting the strict emission standards of the European Union (EU) on the non-road mobile machinery. The object of this article is mainly to explore the effects of intake charge on OFC in a dual-injection SI engine fuelled with gasoline at economical oxygen-fuel ratios. One-dimensional simulation by software GT-Power is used to analyse engine performance and combustion characteristics under three injection strategies, including GDI (only using GDI), P-G (50% PFI and 50% GDI) and PFI (only using PFI). This article will contribute a theoretical basis for implementing OFC technology in ICE, especially dual-injection SI engines.

2. Research methodology

To satisfy the requirement of OFC implementation in practical ICE, the major difficulty is to realise accurate operation and control of combustion process successfully. It is required to establish reliable systems to provide the necessary functions of oxygen feeding, intake organisation, fuel injection, CO_2 separation, CO_2 capture and storage, etc. Regarding implementing the intake charge organisation of OFC mode, the intake system of conventional SI engines should be modified under actual conditions. The two typical oxygen feeding strategies which have been implemented in ICE are shown in Figure 3.

One typical strategy of Figure 3 (a) is that CO_2 and oxygen are fed into a mixing chamber, followed by entering into the engine cylinders without Exhaust Gas Recirculation (EGR) system [48][49]. This strategy is utilised in this simulation work because of its simple design without considering EGR control. The other one in Figure 3 (b) is that oxygen is fed into a mixing chamber and engine cylinders together with a portion of exhaust gases from EGR system [13][14][23][24]. In either of these two strategies, high-pressure bottles or liquefied gas tanks are employed as the oxygen supplement resources. The flow rate of oxygen feeding can be stabilised by Proportion Integration Differentiation (PID) controllers and electrochemical oxygen sensors, leading to the Oxygen Mass Fraction (OMF) management in O_2/CO_2 mixtures. Regarding the control of intake charge temperature in SI engines, an intercooler can be used in practical implementations, leading to a change in the volumetric efficiency.

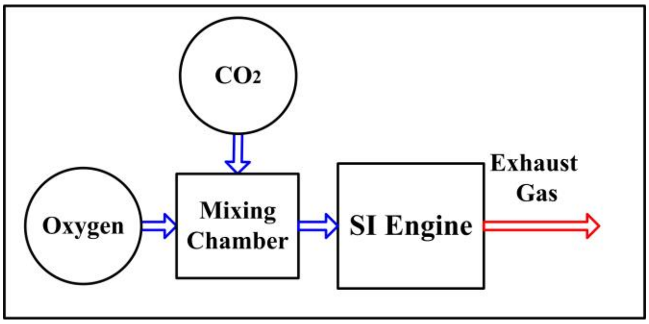

(a)

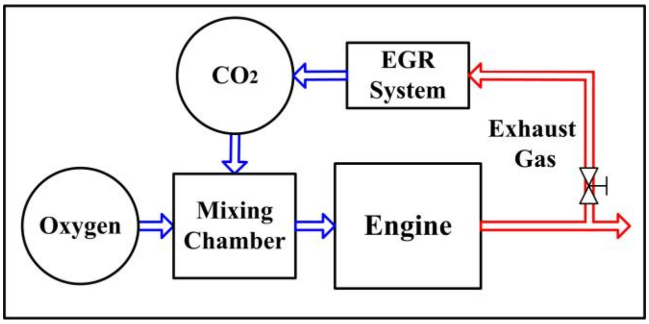

(b)

Figure 3. Schematic of typical oxygen feeding strategies in ICE: (a) oxygen feeding without EGR and (b) oxygen

feeding with EGR

The research selected a typical engine operating condition, which is a medium load of 6 bar Brake Mean Effective Pressure (BMEP) at the engine speed of 2000 revolutions per minute (rpm). In order to clearly illustrate the approach of this research, a flow chart is depicted in Figure 4. First, experimental data of 2000 rpm-6 bar BMEP condition should be collected from a dual-injection engine testbed under CAC mode. Then, the simulation model of this research is available to be verified. After that, engine performance is to be simulated under OFC mode by replacing nitrogen with CO_2, followed by exploring the effects of intake charge under three injection strategies (GDI, P-G and PFI), including varying intake temperature and OMF.

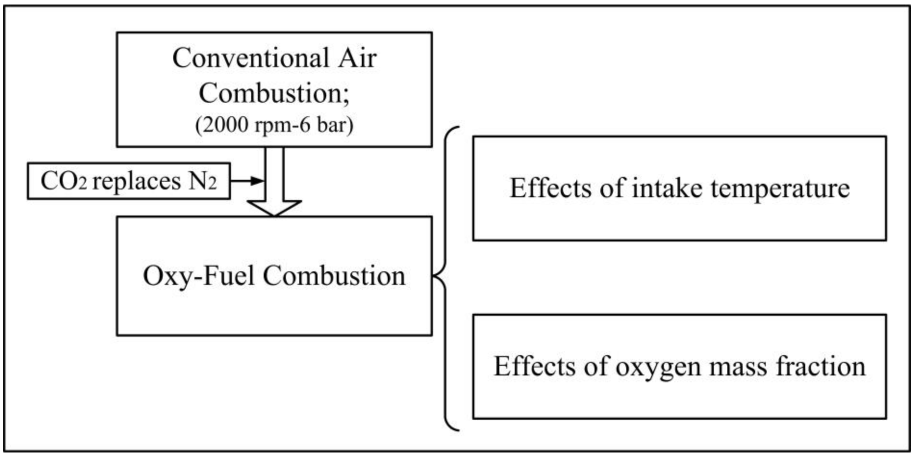

Figure 4. Flow chart of research approach

To help reflect and analyse the combustion characteristics, some key parameters are introduced in this work. Brake Specific Fuel Consumption (BSFC) and Brake Specific Oxygen Consumption (BSOC) is used to evaluate the rate of fuel and oxygen consumption, respectively. Lambda_{O2} is used to represent the oxygen-fuel ratio as equation (2).

$$lambda_{O2} = \frac{\tau_O}{\tau_{ost}} \tag{2}$$

Here, τ_O (kg/h) and τ_{ost} (kg/h) is oxygen mass flow rate under the actual operating condition and stoichiometric condition, respectively.

Besides, φ_{CA10}, φ_{CA50} and φ_{CA90} are introduced to denote the Crank Angle (CA) where 10%, 50% and 90% of the total heat has been released, respectively. Ignition delay (θ_F) denotes the period between spark timing and φ_{CA10}, and combustion duration (θ_C) denotes the period between φ_{CA10} and φ_{CA90}.

3. Engine specifications and experimental facilities

A downsized turbocharged dual-injection engine which specifications are listed in Table 2 is used in this study. Figure 5 depicts the schematic of the engine testbed. An electrical dynamometer is coupled with engine's crankshaft to measure speed, torque and power output. A programmable Electronic Control Unit (ECU) accompanying software INCA can alter the fuel injection ratio of GDI and PFI in real-time. The spark timing is optimised to be the minimum advance for Maximum Brake Torque (MBT) or Knock Limited Spark Advance (KLSA).

The transient cylinder pressure data is detected by piezo-electric pressure transducers (AVL-GH13Z) and a crank encoder (Kistler 2614CK1), followed by amplifying through a Kistler 5018A charge amplifier, then recorded and analysed by an AVL 641combustion analyser. A lambda meter (ETAS LA4) is used to measure the overall air-fuel ratio. The uncertainties of the measured parameters in the test are shown in Table 3 by the root mean square method provided by Holman [50]. To reduce the test error, cylinder pressure data is recorded as an average of 200 consecutive cycles. The overall air-fuel equivalence ratio (lambda), coolant and intercooler output temperature are held constant at 1 ± 0.01, 298 ± 2 K and 358 ± 2 K, respectively.

Table 2. Engine specifications

Items	Content
Engine type	four-cylinder, four-stroke

Bore × Stroke (mm)	82.5 × 92
Displacement (L)	2.0
Injection type	Dual-injection system (PFI plus GDI)
Intake type	Turbocharged
Compression ratio	9.6:1
Rated speed (rpm)	5500
Rated power (kW)	160
Maximum Torque (N·m)	320

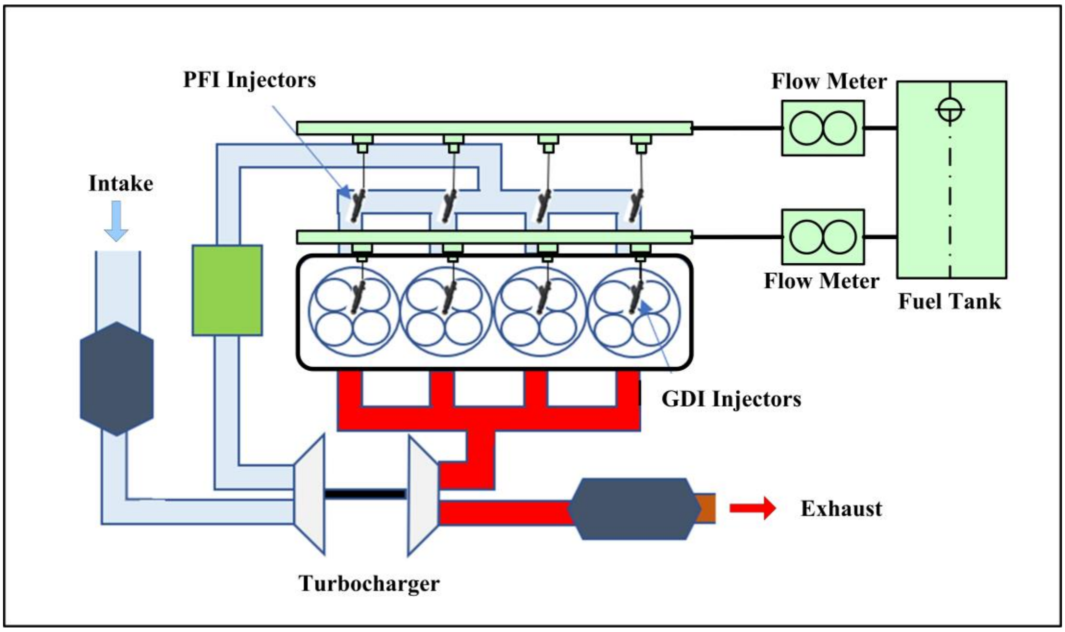

Figure 5. Schematic diagram of engine testbed

Table 3. Uncertainties of measured parameters

Measured Parameters	Uncertainty (%)
Engine speed	± 0.1
BMEP	± 0.1
BSFC	± 0.2
Pressure	± 0.1
Crank angle	± 0.1
Lambda	± 0.3
Coolant temperature	± 0.4
Intercooler output temperature	± 0.4

4. Model description and validation

4.1. Model description

The model is established using GT-Power software, which is one of the most popular simulation tools in academic research of SI engines [51][52][53][54]. The 'SI turbulent flame combustion model' and 'Woschni model' are selected and set up for the sub-model of combustion and heat transfer. Some basic formulas are listed as follows [55][56].

$$S_L = S_{L,0}(\frac{T_u}{T_{ref}})^{\alpha}(\frac{p}{p_{ref}})^{\beta} = (B_m - B_{\emptyset}(\emptyset - \emptyset_m)^2)\left(\frac{T_u}{T_{ref}}\right)^{\alpha}\left(\frac{p}{p_{ref}}\right)^{\beta} f(D) \quad (3)$$

$$Q_W = \int_0^{cycle} \sum_i h\, A_i(T - T_{wi})d\varphi \quad (4)$$

$$h = 110d^{-0.2}P^{0.8}T^{-0.53}[C_1 c_m + C_2 \frac{V_S T_1}{P_1 V_1}(P - P_0)]^{0.8} \quad (5)$$

Here, S_L denotes instantaneous laminar flame speed. $S_{L,0}$ denotes laminar flame speed at 298 K and 101.325 kPa. B_m denotes maximum laminar speed; $B_{\emptyset}$ denotes laminar speed roll-off value; $\emptyset$ denotes in-cylinder equivalence ratio; $\emptyset_m$ denotes equivalence ratio at maximum speed. T_u denotes unburned gas temperature; T_{ref} denotes 298 K; p denotes pressure; p_{ref} denotes 101.325 kPa; α denotes temperature exponent; β denotes pressure exponent. $f(D)$ denotes dilution effect.

Q_W denotes total heat transferred; h denotes heat transfer coefficient; A_i denotes heat absorbing areas of the surfaces; T denotes in-cylinder mean gas temperature; T_{wi} denotes mean surface temperature of A_i; φ denotes CA; d denotes cylinder bore diameter; P denotes cylinder pressure; C_1 denotes a constant related to airflow velocity coefficient; C_2 denotes a constant related to combustion chamber; c_m denotes mean piston speed; V_S denotes cylinder volume; T_1, P_1 and V_1 each denotes cylinder temperature, pressure and volume at the beginning of compression stroke. P_0 denotes cylinder pressure when the engine is started.

Besides, regarding flow object of this model, the cylinder volume V of any CA can be calculated according to the cylinder geometry as Figure 6. The formulas about calculating instantaneous V are as follows.

$$c = \frac{S}{2}[C_R + 1 - cos\theta - ({C_R}^2 + sin^2\theta)^{1/2}] \quad (6)$$

$$V = V_c + \frac{\pi B^2}{4}c = \frac{\pi B^2}{4}\{\frac{S}{C_R - 1} + \frac{S}{2}[C_R + 1 - cos\theta - ({C_R}^2 + sin^2\theta)^{1/2}]\} \quad (7)$$

Here, c denotes piston clearance height; S denotes the stroke; C_R denotes the compression ratio; θ denotes crank CA; V denotes cylinder volume; V_c denotes clearance volume; B denotes cylinder bore diameter.

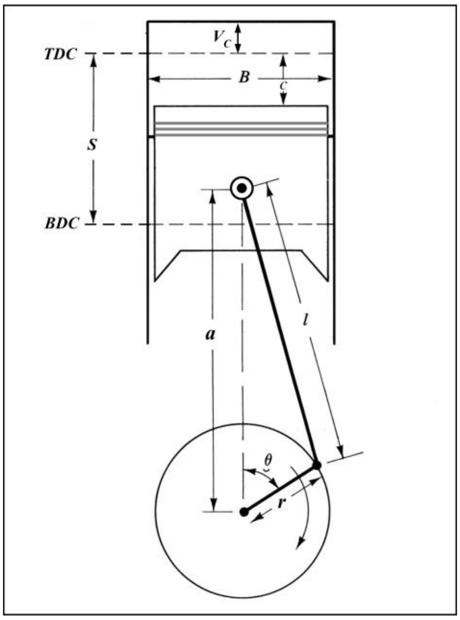

Figure 6. Schematic view of engine cylinder

4.2 Model validation

Figure 7 and Figure 8 present the comparisons of cylinder pressures, in-cylinder temperature and HRR between experimental and simulation results at 2000 rpm-6 bar under CAC mode. It can be seen that the trends of all the curves are quite close between experiment and simulation under each injection strategy. The height and position for all the curves' peaks are accurately predicted. It demonstrates that the model is fully capable of providing predictions in combustion characteristics. Besides, the time-step sensitivity validation of this model is also performed to ensure the accuracy in the calculation results.

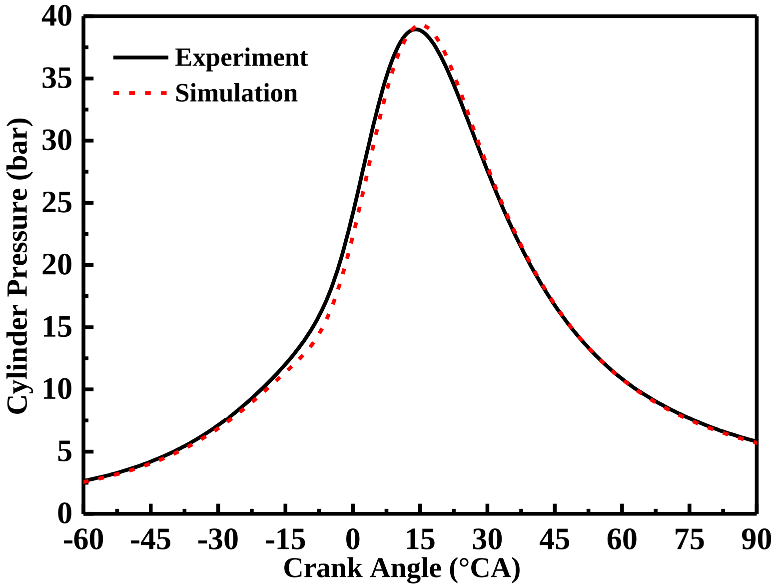
Experiment
Simulation
Cylinder Pressure (bar)
Crank Angle (°CA)
0
5
10
15
20
25
30
35
40
-60
-45
-30
-15
0
15
30
45
60
75
90

(a) GDI

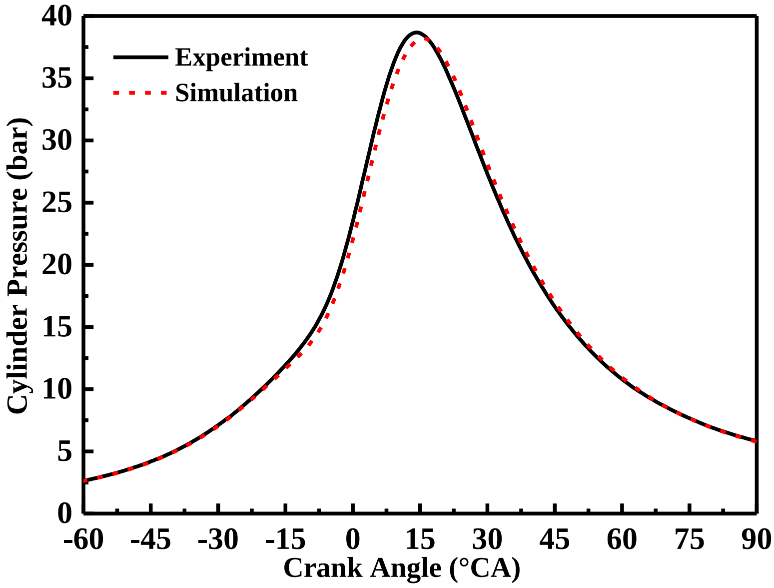
Experiment
Simulation
Cylinder Pressure (bar)
Crank Angle (°CA)
0
5
10
15
20
25
30
35
40
-60
-45
-30
-15
0
15
30
45
60
75
90

(b) P-G

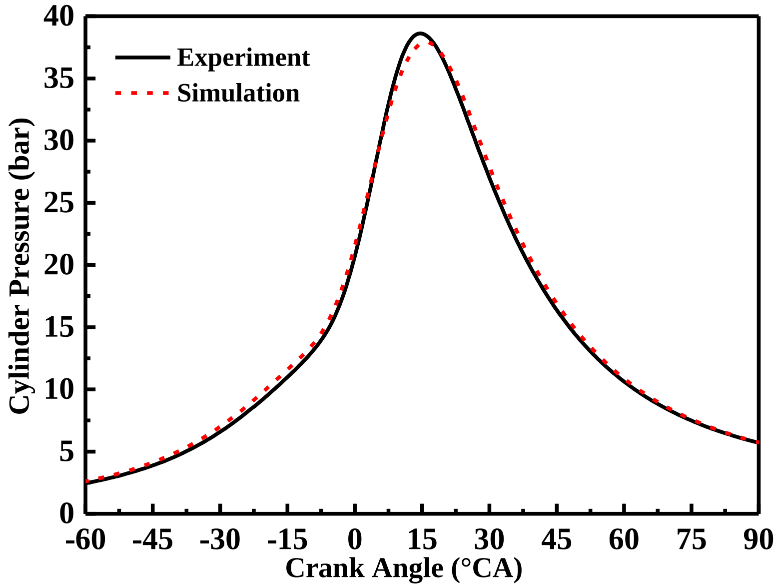

(c) PFI

Figure 7. Comparison of cylinder pressure between experimental and simulation results

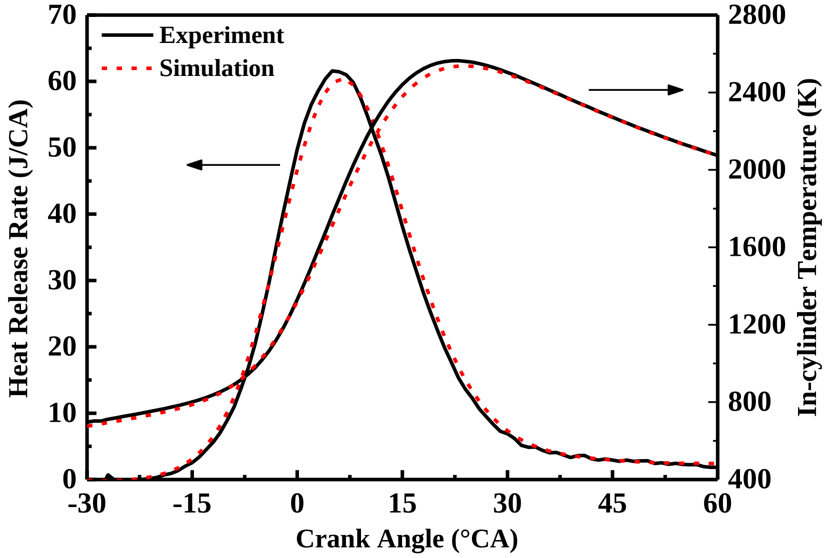

(a) GDI

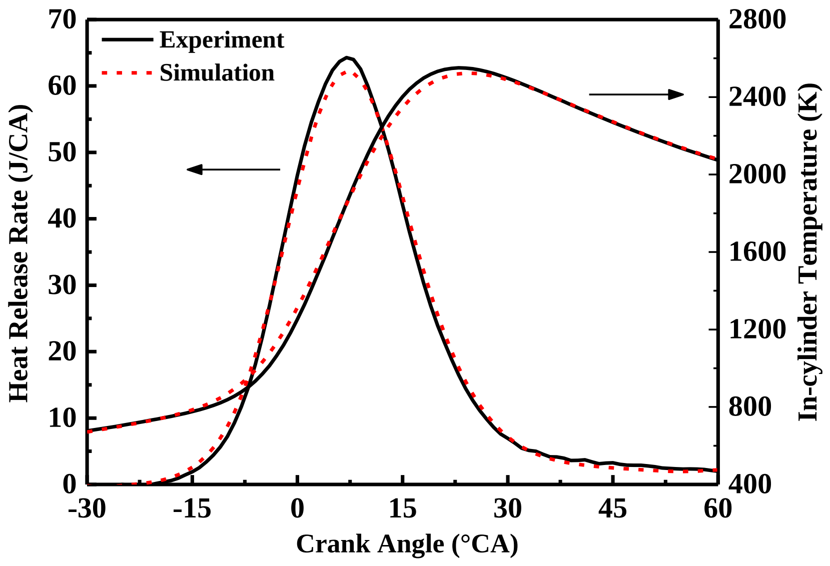

(b) P-G

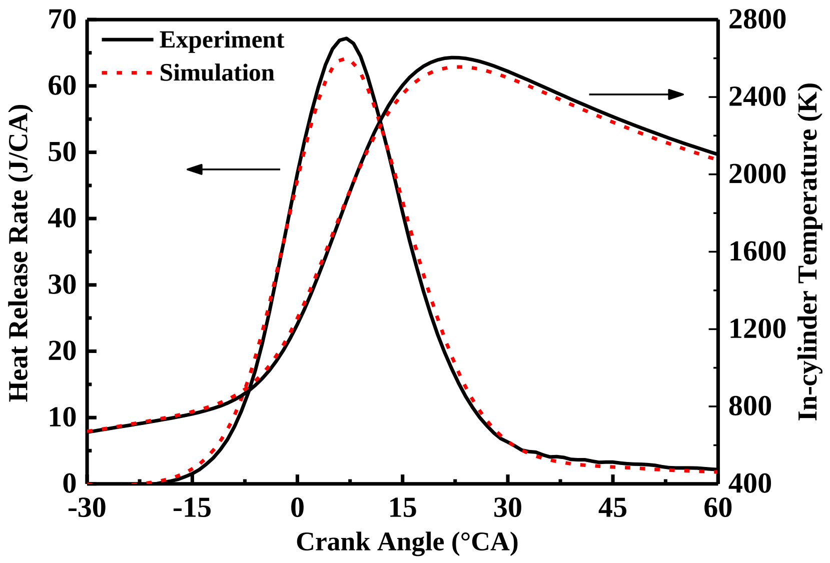

(c) PFI

Figure 8. Comparisons of in-cylinder temperature and HRR between experimental and simulation results

5. Results and discussion

5.1 Evaluation of OFC performance with fixed OMF and intake temperature

As the intake changes from air to oxygen and CO_2, engine combustion is transformed into OFC mode. To make the study purpose explicit under OFC mode, during the sweep of spark timings in this section, the throttle opening angle, intake temperature and OMF are held constant with CAC mode.

As shown in Figure 9, the effects of spark timing on BMEP under OFC includes the following features. First of all, there is a considerable reduction in BMEP from CAC to OFC regardless of injection strategies. The maximum BMEP is each 5.671 bar, 5.649 bar and 5.646 bar for GDI, P-G and PFI, which is 5.48 %, 5.85% and 5.9% less than 6 bar, respectively. This is mainly because that compared to CAC mode, the thermal diffusivity of inert gas (CO_2) is much lower under OFC, which leads to a significant reduction for flame transmission and heat transfer during the combustion process [57][58][59][60]. Second, a correct spark timing is also very important to the performance of BMEP under OFC mode. A marked decline can be caused by further advancing or retarding spark timing. Third, maximum BMEP from high to low in order is that of GDI, P-G and PFI.

The engine performance can be further explained by the variation of combustion phasing characterised by φ_{CA50}, θ_F and θ_C. As shown in Figure 10 and Figure 11, although the general tendency over sweeping spark timings is almost the same, there are still some minor differences among the three injection strategies. Under PFI strategy, the MBT timing which helps obtain maximum brake torque output is postponed by 2 ºCA compared to GDI and P-G. For a given spark timing, the φ_{CA50}, θ_F and θ_C of PFI are the lowest among the three injection strategies, and those of GDI conditions are the highest. It can be attributed to the discrepancies in the gas-fuel mixture approach of different injection strategies. Under PFI conditions, fuel is sprayed into the inlet manifolds to mix with incoming air. It allows a longer period for gas-fuel mixture, leading to a more homogenous in-cylinder environment, promoting flame development.

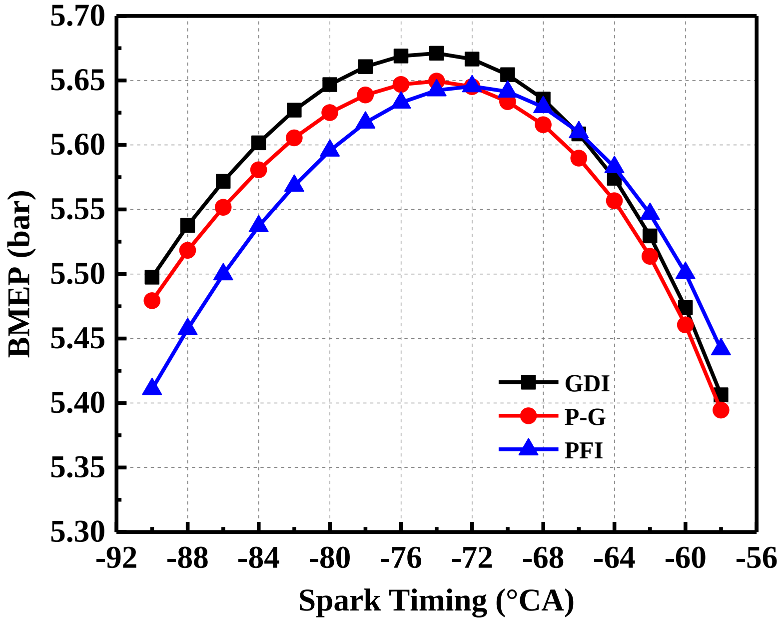

Figure 9. Effects of spark timing on BMEP

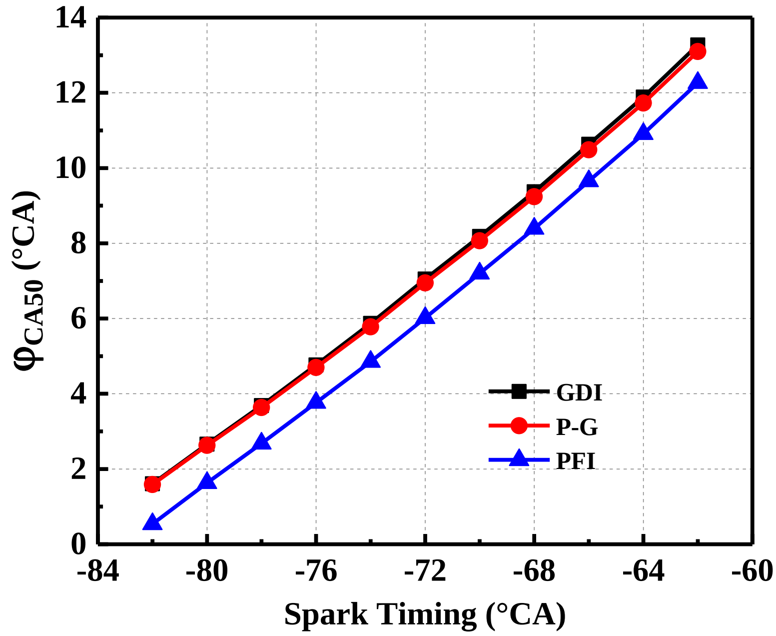

Figure 10. Effects of spark timing on φ_{CA50}

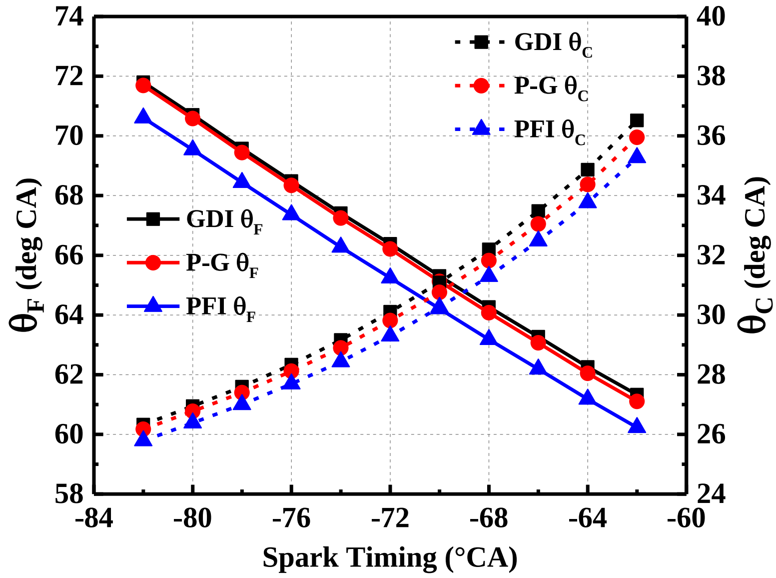

Figure 11. Effects of spark timing on θ_F and θ_C

5.2 Effects of intake temperature on OFC performance

The variation in the BMEP and cylinder pressure at Inlet Valve Closed (IVC) timing with varying intake temperature are presented in Figure 12. Meantime, the throttle opening angle is held constant, and MBT spark timing is applied to all conditions.

It can be observed that BMEP shows a monotonic decrease with increasing intake temperature regardless of injection strategies. The maximum reduction of BMEP can be up to 12.68%, 12.92% and 12.75% for GDI, P-G and PFI, respectively. The loss of BMEP can be attributed to a combined result of two opposite effects. First, with a fixed throttle opening angle and negligible change of turbine speed, volumetric efficiency is considerably deteriorated due to the decreased intake density by increasing intake temperature. The cylinder pressure at IVC timing presents a slight decrease about 0.023 bar as intake temperature increases from 298 K to 378 K. Second, increasing intake temperature can reduce the liquid penetration of fuel spray, decreasing droplet size and spray residence time, leading to a small benefit in vaporisation and atomisation. This will promote more complete combustion, but the benefit cannot counteract the negative impacts of reduced volumetric efficiency [61][62][63].

As shown in Figure 13, with the increase of intake temperature from 298 K to 378 K, a negative influence can be observed on the flow rate. The engine intake flow rate has a reduction of 10.17% on average for all the three injection strategies. As OMF is fixed in intake charge components, the oxygen has the same reduction rate with gross engine intake, leading to a significant negative effect on volumetric efficiency and engine performance.

Figure 14 shows the effects of intake temperature on BSFC and BSOC. There is an increase of about 3% in BSFC and BSOC as intake temperature increases from 298 K to 378 K. Regardless of injection strategies, BSFC and BSOC are directly related to the variation of combustion phase. Figure 15 shows that increasing intake temperature can shorten the θ_F and θ_C. Because higher intake temperature can decrease the kinetic energy of fuel spray, leading to a reduction in liquid penetration, droplet size and residence time, thereby promoting combustion acceleration by enhancing vaporization [61][62]. As shown in Figure 16, by increasing intake temperature to 378 K, φ_{CA50} is slightly advanced by 0.76 ºCA, 0.88 ºCA and 0.92 ºCA under GDI, P-G and PFI, respectively. Increasing intake temperature not only results in advance of Heat Release Rate (HRR), but also reduces the magnitude of HRR's peak.

The analysis above reveals that BMEP, BSFC and BSOC are badly deteriorated by the change of volumetric efficiency and combustion phasing as intake temperature increases. Hence, 298K or a normal room temperature can be an optimum value of intake temperature under OFC mode, ensuring no extra efficiency loss.

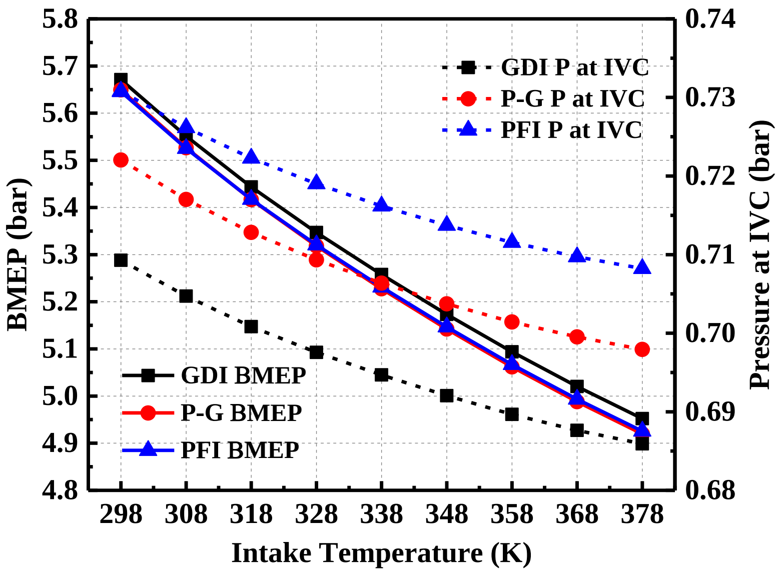

Figure 12. Effects of intake temperature on BMEP and cylinder pressure (at IVC)

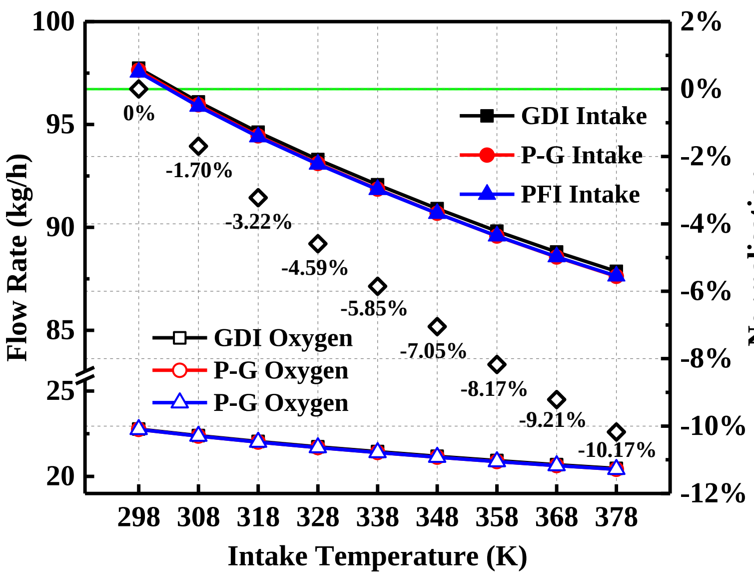

Figure 13. Effects of intake temperature on the mass flow rate of intake and oxygen

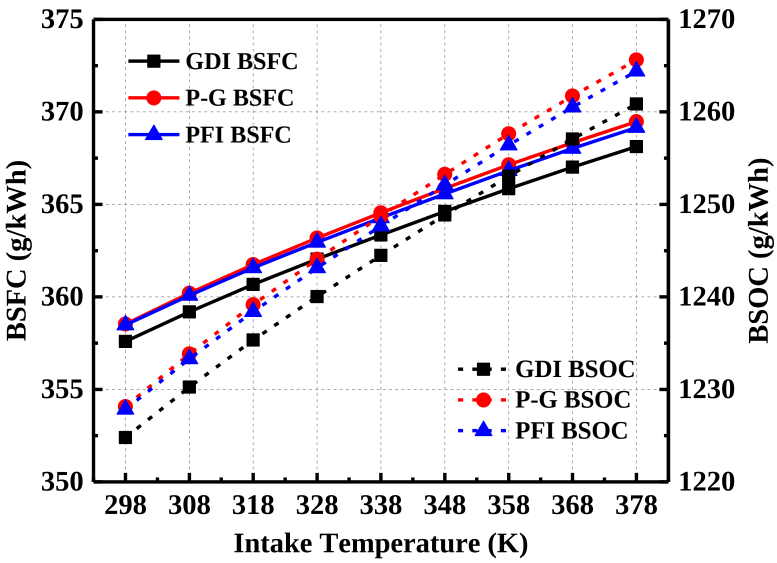

Figure 14. Effects of intake temperature on BSFC and BSOC

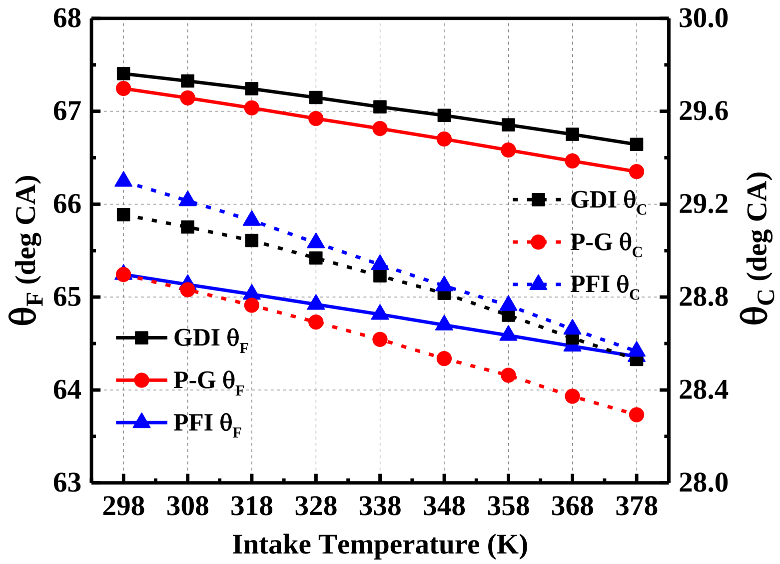

Figure 15. Effects of intake temperature on θ_F and θ_C

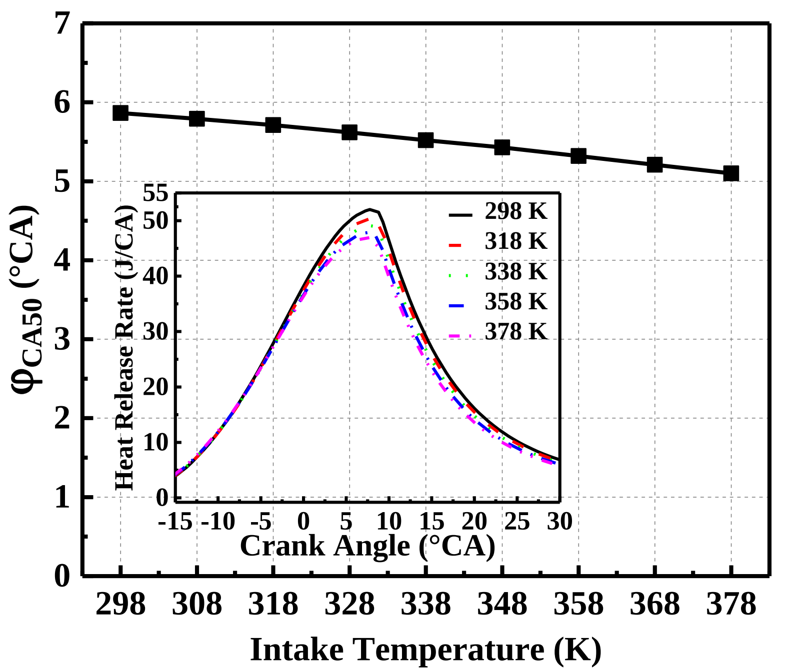

(a) GDI

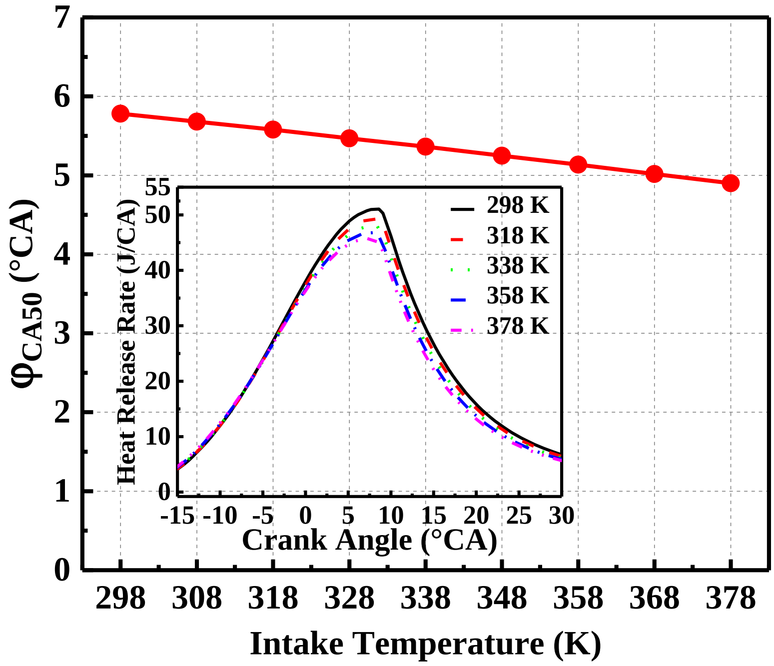

(b) P-G

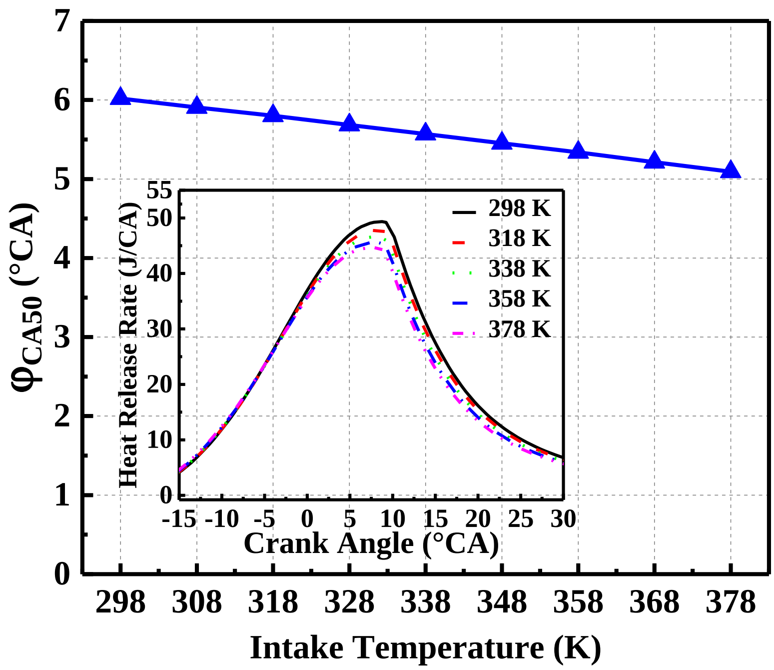

(c) PFI

Figure 16. Effects of intake temperature on φ_{CA50} and HRR

5.3 Effects of OMF on OFC performance

By replacing nitrogen, CO_2 plays a role as an inert gas in the implementation of OFC. Hence, the mass ratio of oxygen and CO_2 will be a crucial influence factor for engine performance and combustion characteristics. In this section, the effects of OMF will be presented and analysed in detail. As this study focuses on theoretical study combines with practical implementations, OMF is set to a range from 23.3% to 29% to ensure the engine operating at economical oxygen-fuel ratios. The details of investigative study cases are shown in Table 4. Meantime, the throttle opening angle is held constant, and intake temperature is kept at 298 K. MBT spark timing is used to all conditions for optimising BMEP or thermal efficiency.

Table 4. Study conditions of intake components

Case	Oxygen mass fraction (%)	CO_2 mass fraction (%)	$Lambda_{O2}$	Lambda (overall)	Intake temperature (K)
1	23.3	76.7	1	1	298
2	25	75	1.073	1	298
3	27	73	1.159	1	298
4	29	71	1.245	1	298

The variation of BMEP with increasing OMF is presented in Figure 17. There is a similar tendency that BMEP has a small increment by increasing OMF under all injection strategies. With the increase of OMF from 23.3% to 29%, the gross growth rate of BMEP is each 0.97%, 1.14% and 1.25% for GDI, P-G and PFI. Even though the increment of BMEP under PFI is a bit higher, but BMEP of GDI is most prominent for any given OMF condition. This is mainly because cooling effect and volumetric efficiency can be enhanced when fuel is directly injected into cylinder chamber under GDI strategy. The maximum BMEP under 29% OMF is 5.726 bar, which is still 0.274 bar less than CAC under the same throttle opening angle. It implies that it is a challenge to achieve the same power output of CAC under OFC mode, largely owing to the lower thermal diffusivity of CO_2 which weakens the flame propagation and heat transfer efficiency [10][11][57][58].

Figure 18 shows the effects of OMF on BSFC and BSOC. With OMF increases from 23.3% to 29%, BSFC decreases by 2.42%, 2.55% and 2.62% for GDI, P-G and PFI, respectively. The considerable improvement is mainly because the specific heat ratio can be improved during the power stroke, thereby increasing energy conversion efficiency [56]. In the meantime, a side effect of increasing OMF on oxygen consumption should be weighted. In order to advance understanding of this phenomenon, Figure 19 and Figure 20 show some key intake and combustion parameters.

In Figure 19, with the OMF increases to 29%, the oxygen flow rate increases by 22.68% on average for all the three injection strategies. Engine intake flow rate slightly reduces by 1.44% on average, mainly because oxygen density is much lighter than CO_2. The cylinder pressure at IVC timing presents a steady trend, slightly affecting the engine performance and combustion characteristics.

Figure 20 shows the effects of OMF on maximum cylinder pressure, maximum in-cylinder temperature and θ_C. With OMF increases from 23.3% to 29%, a good agreement can be observed in the variation of these parameters under all injection strategies. The cylinder pressure and in-cylinder temperature are increased. It is because as OMF increases, a relatively large amount of oxygen enters into the combustion chamber, enabling the combustion to be more efficient for per unit mass of fuel under the lean fuel-oxygen mixture ($lambda_{O2} > 1$). Simulation results also show θ_C is prolonged by increasing OMF. This is mainly because of the impact of lean fuel-oxygen mixture conditions [56][64][65].

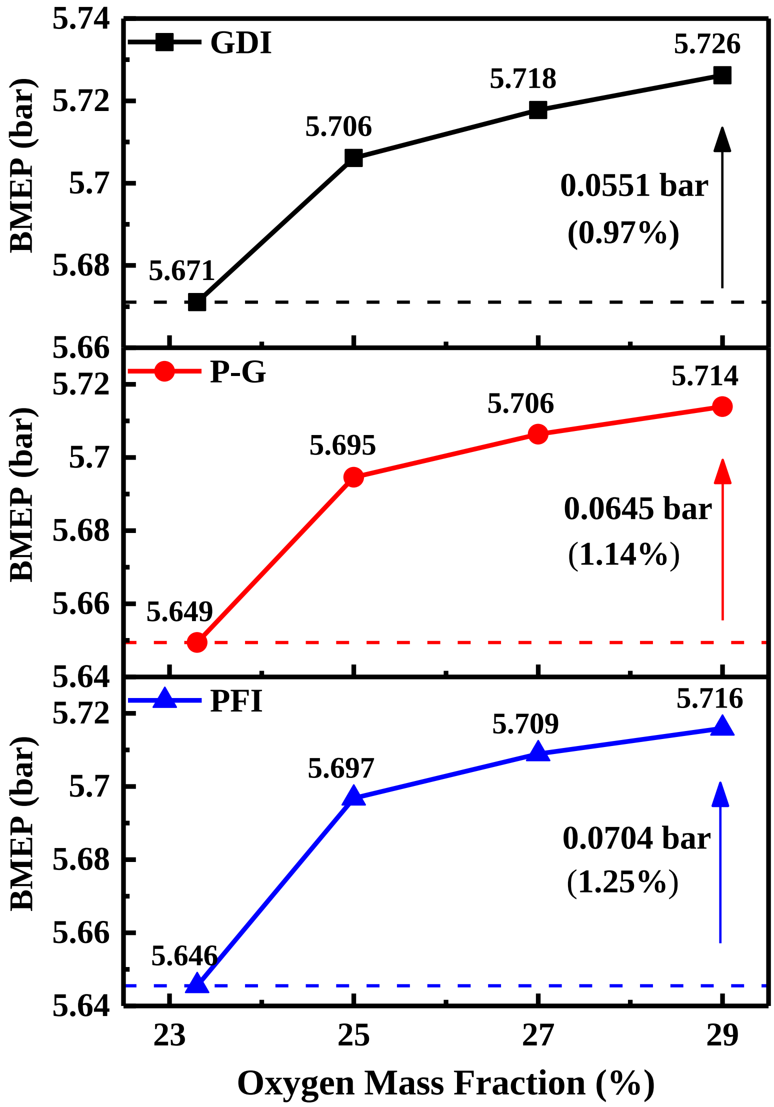

Figure 17. Effects of OMF on BMEP

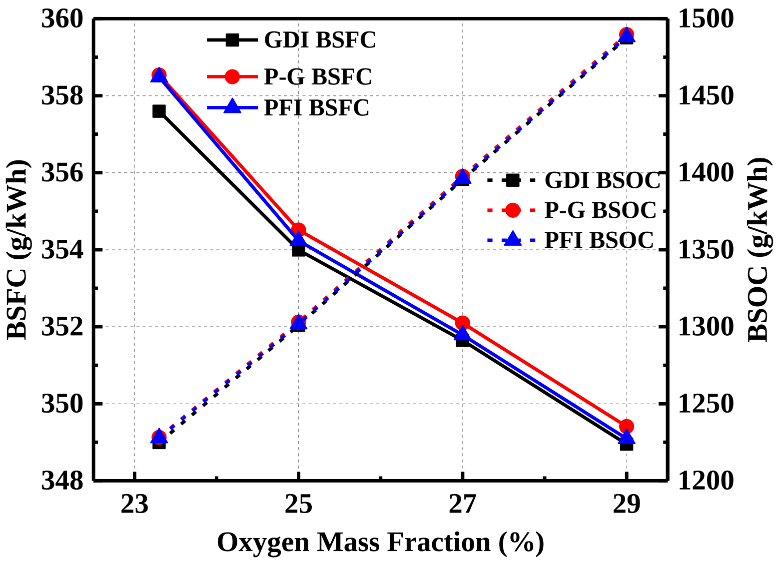

Figure 18. Effects of OMF on BSFC and BSOC

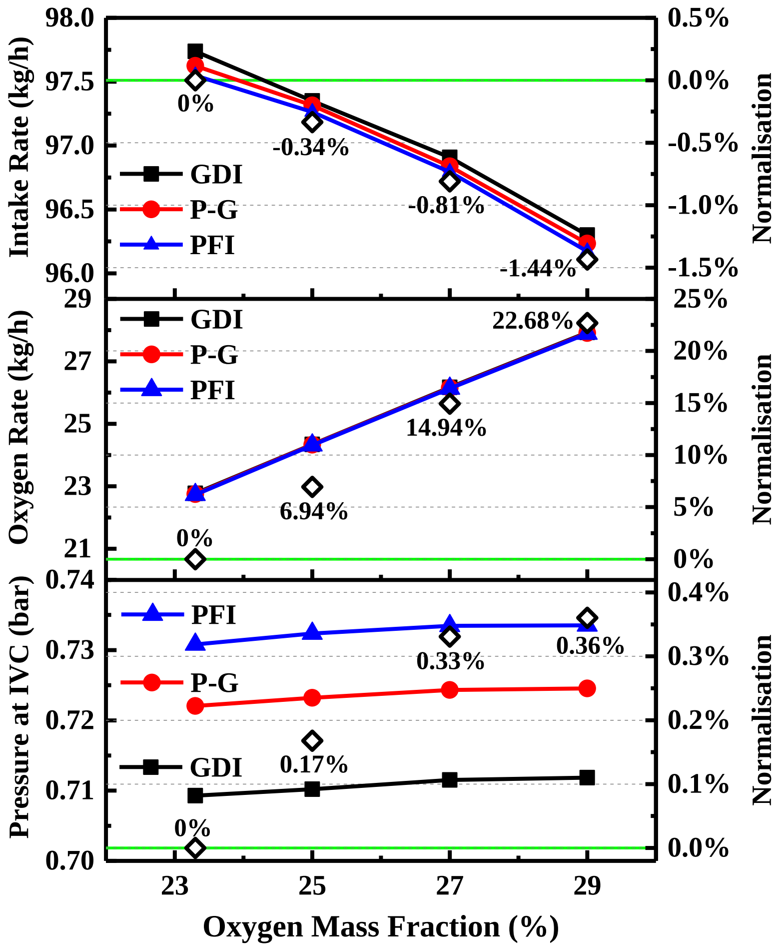

Figure 19. Effects of OMF on intake flow rate, oxygen flow rate and cylinder pressure (at IVC)

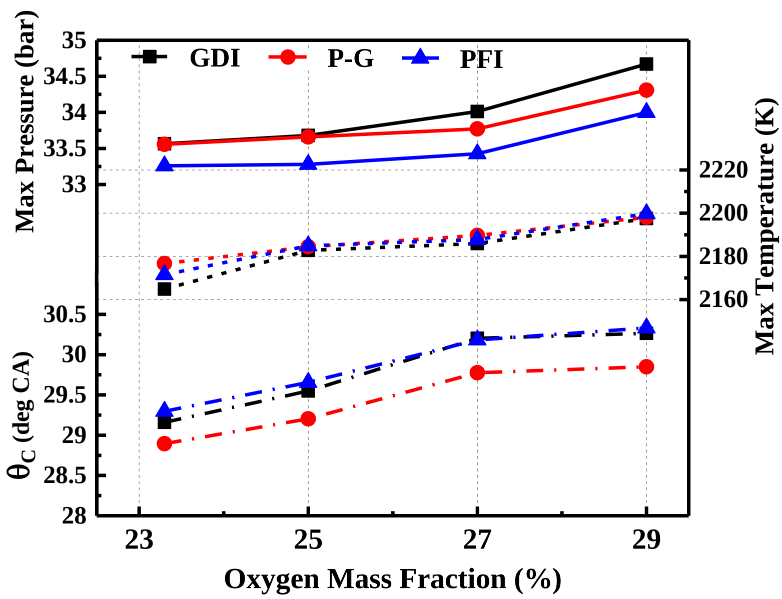

Figure 20. Effects of OMF on maximum cylinder pressure, maximum in-cylinder temperature and θ_C

Conclusion

In this work, a numerical study was conducted in a dual-injection SI engine fuelled with gasoline at economical oxygen-fuel ratios. The effects of intake temperature and OMF on OFC characteristics of dual-injection SI engine are explored for the first time under three injection strategies, including GDI, P-G and PFI. The findings of this work are capable of providing a valuable resource to help understand the effects of intake charge on dual-injection SI engines under OFC mode. The findings are also helpful to provide a foundation to future works, which are about to further explore the potential to improve engine efficiency of an OFC dual-injection SI engine. The main results of this work can be summarised as follows:

1. Under OFC mode with fixed OMF and intake temperature, the maximum BMEP is each 5.671 bar, 5.649 bar and 5.646 bar for GDI, P-G and PFI strategy, which leads to a considerable decrease compared to CAC. The MBT timing of PFI is postponed by 2 ºCA compared to GDI and P-G. φ_{CA50}, θ_F and θ_C of PFI are the lowest among three injection strategies.
2. With intake temperature increases from 298 K to 378 K, BMEP, BSFC and BSOC are badly deteriorated by the change of volumetric efficiency and combustion phasing. The engine intake flow rate has a reduction of 10.17% on average. The reduction of BMEP can be up to 12.68%, 12.92% and 12.75% for GDI, P-G and PFI, respectively. Meantime, there is an increase of about 3% in BSFC and BSOC.
3. By increasing OMF, θ_C is prolonged. Cylinder pressure and in-cylinder temperature are increased. With OMF increases from 23.3% to 29%, the benefits on engine torque and fuel efficiency are more evident under GDI strategy. The gross growth rate of BMEP is each 0.97%, 1.14% and 1.25% for GDI, P-G and PFI. BSFC has a saving rate of 2.42%, 2.55% and 2.62% for GDI, P-G and PFI, respectively.

Acknowledgement

This work is financially supported by the Interreg North-West Europe (Project No. NWE553).

Reference

[1] Figueroa J D, Fout T, Plasynski S, et al. Advances in CO_2 capture technology—the US Department of Energy's Carbon Sequestration Program. International journal of greenhouse gas control, 2008, 2(1): 9-20.
[2] Kanniche M, Gros-Bonnivard R, Jaud P, et al. Pre-combustion, post-combustion and oxy-combustion in thermal power plant for CO_2 capture. Applied Thermal Engineering, 2010, 30(1): 53-62.
[3] Mondal M K, Balsora H K, Varshney P. Progress and trends in CO_2 capture/separation technologies: a review. Energy, 2012, 46(1): 431-441.
[4] Koytsoumpa E I, Bergins C, Kakaras E. The CO_2 economy: Review of CO_2 capture and reuse technologies. The Journal of Supercritical Fluids, 2018, 132: 3-16.
[5] Anwar M N, Fayyaz A, Sohail N F, et al. CO_2 capture and storage: a way forward for sustainable environment. Journal of environmental management, 2018, 226: 131-144.
[6] Reitz R D, Ogawa H, Payri R, et al. IJER editorial: the future of the internal combustion engine. International Journal of Engine Research, 2020, 21(1) 3–10.
[7] Lyu Y, Siddique A R M, Majid S H, et al. Electric vehicle battery thermal management system with thermoelectric cooling. Energy Reports, 2019, 5: 822-827.
[8] Zheng G, Peng Z. Life Cycle Assessment (LCA) of BEV's environmental benefits for meeting the challenge of ICExit (Internal Combustion Engine Exit). Energy Reports, 2021, 7: 1203-1216.
[9] Yaverbaum, L. Fluidized Bed Combustion of Coal and Waste Materials; Noyes Data Corp.: Park Ridge, NJ, 1977.
[10] Stephen R. An introduction to combustion: concepts and applications. McGraw-Hill, 1996.
[11] Wall T, Liu Y, Spero C, et al. An overview on oxyfuel coal combustion—State of the art research and technology development. Chemical engineering research and design, 2009, 87(8): 1003-1016.
[12] Chen L, Yong S Z, Ghoniem A F. Oxy-fuel combustion of pulverized coal: Characterization, fundamentals, stabilization and CFD modeling. Progress in energy and combustion science, 2012, 38(2): 156-214.
[13] Thompson R V, Fowler A. Development of a depth independent closed cycle diesel engine. Offshore Technology Conference. Offshore Technology Conference, 1981.
[14] Shaw R, Oman H. Non-air working fluids for closed-cycle diesel engines. Proc., Intersoc. Energy Convers. Eng. Conf.;(United States). The Boeing Company, Seattle, Washington, 1983, 2(CONF-830812-).
[15] Zhang J B, and Zhu W Q, Simulating computation and experimental study of the closed-cycle diesel engine. Journal of Engineering Thermophysics, 1988 (1): 6.
[16] Wu H W, Shu C T. Effects of operating parameters on steady and transient behaviors of a closed cycle diesel engine. Energy conversion and management, 2006, 47(15-16): 2070-2080.
[17] Wu H W, Wu Z Y, Yang J Y, et al. Combustion characteristics of a closed cycle diesel engine with different intake gas contents. Applied thermal engineering, 2009, 29(5-6): 848-858.

[18] Wu H W, Wang R H, Chen Y C, et al. Influence of port-inducted ethanol or gasoline on combustion and emission of a closed cycle diesel engine. Energy, 2014, 64: 259-267.

[19] Mobasheri R, Aitouche A, Peng Z, et al. Influence of Oxy-Fuel Combustion on Engine Operating Conditions and Combustion Characteristics in a High Speed Direct Injection (HSDI) Diesel Engine under Homogenous Charge Compression Ignition (HCCI) Mode. SAE Technical Paper, 2020.

[20] Mobasheri R, Aitouche A, Peng Z, et al. A numerical study of the effects of oxy-fuel combustion under homogeneous charge compression ignition regime. International Journal of Engine Research, 2021: 1468087421993359.

[21] Li X, Peng Z, Ajmal T, et al. A feasibility study of implementation of oxy-fuel combustion on a practical diesel engine at the economical oxygen-fuel ratios by computer simulation. Advances in Mechanical Engineering, 2020, 12(12): 1687814020980182.

[22] Bilger R W. Zero release combustion technologies and the oxygen economy. Fifth International Conference on Technologies and Combustion for a Clean Environment, Lisbon, Portugal, Jul. 1999: 12-15.

[23] Bilger R W, Wu Z. Carbon capture for automobiles using internal combustion Rankine cycle engines. Journal of Engineering for Gas Turbines and Power, 2009, 131(3).

[24] Yu X, Wu Z, Fu L, et al. Study of combustion characteristics of a quasi internal combustion rankine cycle engine. SAE Technical Paper, 2013.

[25] Yu X, Wu Z, Wang C, et al. Study of the combustion and emission characteristics of a quasi ICRC engine under different engine loads. SAE Technical Paper, 2014.

[26] Fu L, Wu Z, Li L, et al. Effect of Water Injection Temperature on Characteristics of Combustion and Emissions for Internal Combustion Rankine Cycle Engine. SAE Technical Paper, 2014.

[27] Wu Z J, Yu X, Fu L Z, et al. A high efficiency oxyfuel internal combustion engine cycle with water direct injection for waste heat recovery. Energy, 2014, 70: 110-120.

[28] Wu Z, Yu X, Fu L, et al. Experimental study of the effect of water injection on the cycle performance of an internal-combustion Rankine cycle engine. Proceedings of the Institution of Mechanical Engineers, Part D: Journal of Automobile Engineering, 2014, 228(5): 580-588.

[29] Fu L, Wu Z, Yu X, et al. Experimental investigation of combustion and emission characteristics for internal combustion rankine cycle engine under different water injection laws. Energy Procedia, 2015, 66: 89-92.

[30] Jiang C, Xu H, Srivastava D, et al. Effect of fuel injector deposit on spray characteristics, gaseous emissions and particulate matter in a gasoline direct injection engine. Applied energy, 2017, 203: 390-402.

[31] Li X, Pei Y, Qin J, et al. Effect of ultra-high injection pressure up to 50 MPa on macroscopic spray characteristics of a multi-hole gasoline direct injection injector fueled with ethanol. Proceedings of the Institution of Mechanical Engineers, Part D: Journal of Automobile Engineering, 2018, 232(8): 1092-1104.

[32] Ma H, Li Z, Tayarani M, et al. Model-based computational intelligence multi-objective optimization for gasoline direct injection engine calibration. Proceedings of the Institution of Mechanical Engineers, Part D: Journal of Automobile Engineering, 2019, 233(6): 1391-1402.

[33] Raut A A, Mallikarjuna J M. Effects of direct water injection and injector configurations on performance and emission characteristics of a gasoline direct injection engine: A computational fluid dynamics analysis. International Journal of Engine Research, 2020, 21(8): 1520-1540.

[34] Frommater S, Neumann J, Hasse C. A phenomenological modelling framework for particle emission simulation in a direct-injection gasoline engine. International Journal of Engine Research, 2021, 22(4): 1166-1179.
[35] Wang X, Zhao H. Effect of piston shape design on the scavenging performance and mixture preparation in a two-stroke boosted uniflow scavenged direct injection gasoline engine. International Journal of Engine Research, 2021, 22(5): 1484-1499.
[36] Ikoma T, Abe S, Sonoda Y, et al. Development of V-6 3.5-liter engine adopting new direct injection system. SAE Technical Paper, 2006.
[37] Stein R A, House C J, Leone T G. Optimal use of E85 in a turbocharged direct injection engine. SAE International Journal of Fuels and Lubricants, 2009, 2(1): 670-682.
[38] Wurms R, Jung M, Adam S, et al. Innovative technologies in current and future TFSI engines from Audi. 20th Aachen Colloquium automobile and engine technology, 2011.
[39] Wu X, Daniel R, Tian G, et al. Dual-injection: The flexible, bi-fuel concept for spark-ignition engines fuelled with various gasoline and biofuel blends. Applied Energy, 2011, 88(7): 2305-2314.
[40] Daniel R, Wang C, Xu H, et al. Dual-injection as a knock mitigation strategy using pure ethanol and methanol. SAE International Journal of Fuels and Lubricants, 2012, 5(2): 772-784.
[41] Daniel R, Xu H, Wang C, et al. Gaseous and particulate matter emissions of biofuel blends in dual-injection compared to direct-injection and port injection. Applied energy, 2013, 105: 252-261.
[42] Zhuang Y, Hong G. Primary investigation to leveraging effect of using ethanol fuel on reducing gasoline fuel consumption. Fuel, 2013, 105: 425-431.
[43] Zhuang Y, Hong G. Effects of direct injection timing of ethanol fuel on engine knock and lean burn in a port injection gasoline engine. Fuel, 2014, 135: 27-37.
[44] Zhuang Y, Zhu G, Gong Z, et al. Experimental and numerical investigation of performance of an ethanol-gasoline dual-injection engine. Energy, 2019, 186: 115835.
[45] Wang Z, Liu H, Long Y, et al. Comparative study on alcohols–gasoline and gasoline–alcohols dual-fuel spark ignition (DFSI) combustion for high load extension and high fuel efficiency. Energy, 2015, 82: 395-405.
[46] Liu H, Wang Z, Long Y, et al. Dual-Fuel Spark Ignition (DFSI) combustion fuelled with different alcohols and gasoline for fuel efficiency. Fuel, 2015, 157: 255-260.
[47] Liu H, Wang Z, Long Y, et al. Comparative study on alcohol–gasoline and gasoline–alcohol Dual-Fuel Spark Ignition (DFSI) combustion for engine particle number (PN) reduction. Fuel, 2015, 159: 250-258.
[48] Hawley J G, Ashcroft S J, Patrick M A. The effects of non-air mixtures on the operation of a diesel engine by experiment and by simulation. Proceedings of the Institution of Mechanical Engineers, 1998, 212(1): 55.
[49] Kang Z, Wu Z, Zhang Z, et al. Study of the combustion characteristics of a HCCI engine coupled with oxy-fuel combustion mode. SAE International Journal of Engines, 2017, 10(3): 908-916.
[50] Holman J P. Experimental methods for engineers. Mc Grawhill, 1966.
[51] Teodosio L, Pirrello D, Berni F, et al. Impact of intake valve strategies on fuel consumption and knock tendency of a spark ignition engine. Applied Energy, 2018, 216: 91-104.
[52] Tornatore C, Bozza F, De Bellis V, et al. Experimental and numerical study on the influence of cooled EGR on knock tendency, performance and emissions of a downsized spark-ignition engine. Energy, 2019, 172: 968-976.

[53] Zhen X, Li X, Wang Y, et al. Effects of the initial flame kernel radius and EGR rate on the performance, combustion and emission of high-compression spark-ignition methanol engine. Fuel, 2020, 262: 116633.

[54] Zhen X, Tian Z, Wang Y, et al. A model to determine the effects of low proportion of hydrogen and the flame kernel radius on combustion and emission performance of direct injection spark ignition engine. Process Safety and Environmental Protection, 2021, 147: 1110-1124.

[55] Woschni, G., A universally applicable equation for the instantaneous heat transfer coefficient in the internal combustion engine. No. 670931. SAE Technical paper, 1967.

[56] Heywood, J.B., "Internal Combustion Engine Fundamentals (2nd edit)." McGraw-Hill, 2018.

[57] Liu H, Zailani R, Gibbs B M. Comparisons of pulverized coal combustion in air and in mixtures of O2/CO2. Fuel, 2005, 84(7-8): 833-840.

[58] Molina A, Shaddix C R. Ignition and devolatilization of pulverized bituminous coal particles during oxygen/carbon dioxide coal combustion. Proceedings of the combustion institute, 2007, 31(2): 1905-1912.

[59] Shaddix C R, Molina A. Particle imaging of ignition and devolatilization of pulverized coal during oxy-fuel combustion. Proceedings of the combustion institute, 2009, 32(2): 2091-2098.

[60] Zhang L, Binner E, Qiao Y, et al. In situ diagnostics of Victorian brown coal combustion in O2/N2 and O2/CO2 mixtures in drop-tube furnace. Fuel, 2010, 89(10): 2703-2712.

[61] Park S H, Kim H J, Lee C S. Comparison of experimental and predicted atomization characteristics of high-pressure diesel spray under various fuel and ambient temperature. Journal of mechanical science and technology, 2010, 24(7): 1491-1499.

[62] Heldmann M, Knorsch T, Wensing M. Investigation of fuel atomization and evaporation of a DISI injector spray under homogeneous charge conditions. SAE International Journal of Engines, 2013, 6(2): 1213-1221.

[63] Lee Z, Kim T, Park S, et al. Review on spray, combustion, and emission characteristics of recent developed direct-injection spark ignition (DISI) engine system with multi-hole type injector. Fuel, 2020, 259: 116209.

[64] Metghalchi M, Keck J C. Burning velocities of mixtures of air with methanol, isooctane, and indolene at high pressure and temperature. Combustion and flame, 1982, 48: 191-210.

[65] Milton B E, Keck J C. Laminar burning velocities in stoichiometric hydrogen and hydrogen-hydrocarbon gas mixtures. Combustion and Flame, 1984, 58(1): 13-22.

Appendix

Abbreviations

BMEP	Brake Mean Effective Pressure
BSFC	Brake Specific Fuel Consumption
BSOC	Brake Specific Oxygen Consumption
CA	Crank Angle
CAC	Conventional Air Combustion
CCDE	Closed Cycle Diesel Engine
CCS	Carbon Capture and Storage
CI	Compression Ignition
CO_2	Carbon Dioxide
DI	Direct Injection

E85	a blend of 15% gasoline and 85% ethanol
ECU	Electronic Control Unit
EGR	Exhaust Gas Recirculation
EPA	Environmental Protection Agency
EU	European Union
GDI	Gasoline Direct Injection
GHG	Greenhouse Gas
HCCI	Homogenous Charge Compression Ignition
HRR	Heat Release Rate
ICE	Internal Combustion Engine
ICRC	Internal Combustion Rankine Cycle
IVC	Inlet Valve Closed
KLSA	Knock Limited Spark Advance
MBT	Maximum Brake Torque
OFC	Oxy-Fuel Combustion
OMF	Oxygen Mass Fraction
PFI	Port Fuel Injection
PID	Proportion Integration Differentiation
P-G	50% Port Fuel Injection and 50% Gasoline Direct Injection
rpm	revolutions per minute
SI	Spark Ignition